photonics

MDPI

Communication

Modeling for Generating Femtosecond Pulses in an Er-Doped Fiber Using Externally Controlled Spectral Broadening and Compression Mechanisms

Mohamed Hemdan Abo-elenein [1,*], Salah Eldeen Ibrahim Hassab Elnaby [1], Amin Fahim Hassan [2] and Afaf Mahmoud Abd-Rabou [2]

[1] Department of Engineering Applications of Lasers, National Institute of Laser Enhanced Sciences, Cairo University, Giza 12613, Egypt; selnaby@niles.edu.eg
[2] Department of Physics, Faculty of Science, Helwan University, Ain Helwan, Cairo 11792, Egypt; aminfahim@science.helwan.edu.eg (A.F.H.); afaf_mahmoud@science.helwan.edu.eg (A.M.A.-R.)
* Correspondence: m_aboelenein@yahoo.com

Abstract: A model for generating femtosecond laser pulses from a low-power mode-locked laser of moderate temporal half-width was proposed. This was achieved by injecting the pulse into a single-mode inverted-populated Er-doped fiber where self-focusing and absorption were avoided. To initiate spectral broadening, the pulse was phase-modulated by subjecting a part of the fiber to an electric field of suitable intensity and frequency generated into a circular capacitor. To stimulate temporal compression, the phase-modulated pulse was introduced into a combination of two prism sets located symmetrically with respect to the *x*-axis. After passing the pulse through the first prism set, its spectral components were spatially separated in the *y*-axis. The spectral phases were manipulated by redirecting the spectral components through a slab cross-section that was subjected to a spatially modulated DC electric field. After passing the slab, the pulse is directed into the second prism set, where the spectral components were spatially overlapped and propagated outside the compressor with the same slope and dimension as before entering the compressor. Constructive super positioning of the phase-manipulated spectral components gave maximum intensity only at a specified location.

Keywords: external phase modulation; femtosecond laser pulse; kerr effect; pulse compression; spectral phase modulation

Citation: Abo-elenein, M.H.; Hassab Elnaby, S.E.I.; Hassan, A.F.; Abd-Rabou, A.M. Modeling for Generating Femtosecond Pulses in an Er-Doped Fiber Using Externally Controlled Spectral Broadening and Compression Mechanisms. *Photonics* **2022**, *9*, 205. https://doi.org/10.3390/photonics9040205

Received: 18 January 2022
Accepted: 16 March 2022
Published: 22 March 2022

1. Introduction

Since the development of mode-locked lasers, shorter pulse durations have been required for many applications in science, medicine, and engineering. Such applications are given in [1–9]. To direct a conventional laser pulse into a femtosecond region, it is mathematically necessary to broaden its spectral bandwidth. Because this is achievable by applying nonlinear phenomena to the pulse, different methods for its realization were presented in [10–14]. According to the dispersion relations of the refractive index, the frequency components comprising the spectral bandwidth of the pulse have different velocities. Each frequency will reach an observer at different times, leading either to compressing or expanding the pulse duration. Since most of the materials have a positive-group-delay dispersion (PGDD) that expands the pulse duration, a material of negative-group-delay dispersion (NGDD) is required to reduce its duration. References [15–22] have illustrated different setups for its practical realization. From the above, it is evident that mutual combinations between broadening and compression methods will theoretically yield a temporal compressed pulse. So, for instance, the authors in [23] used nonlinear phenomena to increase the spectral range of a 90 fs laser pulse in a fiber and compressed the broadened pulse by a grating compressor to 30 fs. A pulse compression ratio of 12

(from 5.4 ps to 450 fs) was reported in [24] by using self-phase modulation in a 30 m optical fiber to broaden the spectrum and a grism compressor. The result of a theoretical analysis based on the solution of the nonlinear Schrödinger equation concerning pulse compression ratio and compression pulse quality as a function of fiber length and input pulse intensity was given in [25]. The study was carried out on an optical pulse chirped in a single-mode fiber by self-phase modulation and compressed with a grating compressor. Self-phase modulation in bulk material for spectral broadening the laser pulse and chirped mirror combined with two prisms for its compression was given in [26].

From the previous cited references, it is evident that most of the researchers used:

(1) Powerful laser pulses for internally driving nonlinear phenomena to initiate the spectral broadening of the laser pulse;
(2) Compressors with moveable compressor elements for creating compressed pulses at a desired location.

Aim of the Work

To generate a femtosecond laser pulse from a mode-locked laser pulse of low power and moderate halfwidth, it is necessary to externally stimulate nonlinear phenomena. The present article developed a model for their realization. Section 2.1 is devoted for finding a mathematical expression for an electric field that externally phase-modulates the laser pulse during its propagation in the fiber and a setup for its experimental realization. Section 2.2 is devoted to finding a method for external variation of the spectral optical path lengths. Therefore, the spectral phases are controlled such that the pulse compression occurs at a desired location without movement any of the compressor elements. A suggested setup for the experimental realization is also included.

2. Theory

Erbium-doped fibers (EDF) were chosen for generating femtosecond laser pulses for several reasons. They show high gain, polarization-independent amplification, low intrinsic optical noise [27], stable long-term performance, and possibility of being unidirectionally and bidirectionally pumped [28]. To avoid absorption and self-focusing of the laser pulse, the selected fiber was a single-mode and inverted populated. To achieve the cited goal, the pulses had to be externally spectrally broadened during propagation in the EDF. Two prism sets and a slab (for external manipulation of the spectral phases) were responsible for temporally compressing the spectrally broadened laser pulse.

2.1. Broadening of the Spectral Bandwidth of the Laser Pulse Using an Externally Triggered Phase Modulation

A laser pulse can be coherently spectrally broadened when it is subjected to nonlinear effects either internally through self-phase modulation or externally by amplitude, frequency, or phase modulation. For a small intensity, where self-phase modulation would be ineffective, external induction of wide-range spectral broadening would be required. This was achieved by an external high-frequency electric field that modulated the refractive index of the fiber according to the following equation [29]:

$$n(\Omega) = n_0(\Omega) + n_2 E^2(t), \quad (1)$$

where Ω is the angular frequency of the electric field of the laser pulse, $n_0(\Omega)$ and n_2 are the linear and nonlinear refractive indices of the fiber, respectively, and E(t) is the time-dependent external applied electric field. To create a femtosecond laser pulse, the induced spectral bandwidth ($\Delta\nu$), according to the Heisenberg uncertainty principle, must be in the order of $1/\Delta t$, where Δt is the desired laser-pulse duration. To fulfill this criterion, the nonlinear part of Equation (1), $n_2E^2(t)$, has to be in the order of the linear part $n_0(\Omega)$. This can be achieved by subjecting the fiber to a high frequency and high electric-field strength. This electric field was created by solving the Maxwell's equations within a circular-shaped capacitor in which a part of the fiber was wrapped. The required value of the electric-field

strength was obtained for certain conditions concerning the radius of the capacitor and the frequency of the generator. Due to the considered symmetry, the Maxwell's equations have been written in cylindrical coordinates as: (detailed solution see Appendix A)

$$\frac{\partial E(r,t)}{\partial r} = \mu \frac{\partial H(r,t)}{\partial t}, \tag{2}$$

$$\frac{\partial H(r,t)}{\partial r} + \frac{1}{r} H(r,t) = \varepsilon \frac{\partial E(r,t)}{\partial t}. \tag{3}$$

With

$$H(r,t) = \mathrm{Re}[H(r)\exp(i\omega t)], \tag{4}$$

$$E(r,t) = \mathrm{Re}[E(r)\exp(i\omega t)], \tag{5}$$

it follows after setting Equations (4) and (5) into Equations (2) and (3) and applying some mathematical manipulations,

$$\frac{\partial^2 H(r)}{\partial r^2} + \frac{1}{r}\frac{\partial H(r)}{\partial r} - \frac{1}{r^2} H(r) + \varepsilon\mu\omega^2 H(r) = 0, \tag{6}$$

$$\frac{1}{\mu i\omega}\frac{\partial^2 E(r)}{\partial r^2} + \frac{1}{r}\frac{1}{\mu i\omega}\frac{\partial E(r)}{\partial r} - \varepsilon i\omega E(r) = 0, \tag{7}$$

where $E(r,t)$ and $H(r,t)$ are the spatial and temporal electric and magnetic field strengths, respectively, $E(r)$ and $H(r)$ are the spatial components of the corresponding fields, respectively, and ε and μ are the electric permittivity and magnetic permeability, respectively.

With $\varepsilon\mu\omega^2 = k^2$, the solution of Equations (6) and (7) are given according to [30], by

$$E(r) = AJ_0(kr) + A'Y_0(kr), \tag{8}$$

$$H(r) = BJ_1(kr) + B'Y_1(kr), \tag{9}$$

where J_0 and J_1 are the first kind Bessel functions of zero and first order, respectively, Y_0 and Y_1 are the second kind Bessel functions of zero and first order, respectively, and A and A' as well as B, and B' are integration constants.

To avoid the singularity of Y_0 and Y_1 at $r = 0$, A' and B' were set as equal to zero. To acquire B, Ampere's law was applied:

$$\oint H(r,t)\mathrm{d}\varphi = B\cos(\omega t)J_1(ka)(2\pi a) = \int \frac{\partial}{\partial t} E(r,t)(2\pi r)\mathrm{d}r = I(t), \tag{10}$$

where $\mathrm{d}\varphi$ is an element of the circular path along $H(r)$ with radius r, a is the radius of the capacitor, and $I(t)$ is the feeding current of the capacitor with amplitude I_o.

Accordingly, B and $H(r)$ are determined, respectively, as:

$$B = I_o/[J_1(ka)2\pi a], \tag{11}$$

$$H(r) = [I_o/(2\pi a)][J_1(kr)/J_1(ka)]. \tag{12}$$

From Equation (3) and considering Equation (12), $E(r)$ is calculated as follows:

$$E(r) = I_o k J_0(kr)/[(i\omega\varepsilon)\,(2\pi a)J_1(ka)], \tag{13}$$

With $A = I_o k/[(i\omega\varepsilon)(2\pi a)J_1(ka)]$, the relation between A and B is as follows:

$$B = iA\sqrt{\varepsilon/\mu}, \tag{14}$$

and the real parts of $E(r,t)$ and $H(r,t)$ can be written, respectively as

$$\mathrm{Re}[E(r,t)] = \mathrm{Re}[AJ_0(kr)\exp(i\omega t)] = I_o k J_0(kr)\sin(\omega t)/[(\omega\varepsilon\,(2\pi a)J_1(ka))], \tag{15}$$

$$\mathrm{Re}[H(r,t)] = \mathrm{Re}[iA\sqrt{\varepsilon/\mu}J_1(kr)\exp(i\omega t)] = I_o k\sqrt{\varepsilon/\mu}J_1(kr)\cos\omega t/[\omega\varepsilon\ (2\pi a)J_1(ka)]. \quad (16)$$

From Equations (15) and (16), the time average of the Poynting vector within the capacitor was equal to zero. This result was in accordance with the assumption of the neglected polarization, absorption losses within the fiber, and the radiation into the surrounding. The latter can be achieved by setting the distance between the capacitor plates to be in the order of 1/100 of the wavelength of the modulating electric field. From Equation (15), it was evident that the electric field could attain large values as $J_1(ka)$ approached small values. Since this was possible for a discrete infinite number of (ka) values, we had to choose between those provided easily available frequencies and suitable capacitor dimensions. From the obtained results, the electric-field strength of the laser pulse was phase-modulated according to the following relation:

$$E_{laser}(z,t) = c_1 \exp\left[-c_2((t-t_s)/\Delta t_s)^2\right] \times \exp(i\Omega_0 t)\exp\left[\left(\frac{2\pi i}{\lambda_0}\right)\left(n_0(\Omega)Z + n_2E^2(t)Z_e\right)\right], \quad (17)$$

where $\exp\left[-c_2((t-t_s)/\Delta t_s)^2\right]$ is the time-dependent amplitude of the electric-field strength of the laser pulse to be phase-modulated; t_s and Δt_s are the time of maximum amplitude and temporal width of the electric-field strength of the laser pulse, respectively, Ω_0 and λ_0 are the central vacuum angular frequency and the wavelength of the laser pulse, respectively, $E^2(t)$ is the square of the phase-modulating electric field obtained in Equation (15), which is multiplied by n_2 to be in the order of $n_0(\Omega)$, n_0 and n_2 are the linear and nonlinear refractive indices, respectively, Z is the total length of the fiber; and Z_e is the length of the fiber subjected to the alternating electric field in the capacitor. To avoid sparking within the capacitor, it had to be placed in a grounded container that had been highly evacuated. This container consists of getter material to adsorb gases that were adsorbed on the surface of the material and might be free during the operation. To maintain a constant fiber temperature, the housing has to be subjected to an air-cooled Peltier cooler.

2.1.1. Computations

By keeping the denominator of Equation (15) constant, the fast Fourier transform (FFT) algorithm was applied on Equation (17) at $Z_e = 2$ m for an amplified laser pulse of a temporal maximum amplitude at 1.8 W, duration $\Delta t_s = 1 \times 10^{-7}$ s, $t_s = 4 \times 10^{-7}$ s, $\Omega_0 = 1.2 \times 10^{15}$ 1/s, $\lambda_0 = 1.531$ µm, phase-modulated with electric-field strength 6.8×10^7 V/m, frequencies of 100 MHz, 1.2 GHz, $n_2 = 3.2 \times 10^{-16}$ m^2/V^2 [31], and $n_0(\lambda)$ given by Sellmeier's equation [32].

$n_0{}^2(\lambda) = \left[1 + B_1\lambda^2/\left(\lambda^2 - C_1\right) + B_2\lambda^2/\left(\lambda^2 - C_2\right) + B_3\lambda^2/\left(\lambda^2 - C_3\right)\right]$ with $B_1 = 0.6968$, $B_2 = 0.40817$, $B_3 = 0.8949$, $C_1 = 6.853 \times 10^{-2}$ µm^2, $C_2 = 0.1161 \times 10^{-2}$ µm^2 and $C_3 = 9.914$ µm^2.

2.1.2. Results and Discussion

For computing the Fourier spectrum, the limited computer capacity made it impossible to account for more than 8×10^6 samples within the frequency range of 7×10^{14} – 1.7×10^{15} 1/s for each of the modulating frequencies.

Figure 1 illustrates the modulus of the amplitude spectrum of the electric field of a laser pulse with a maximum power of 1.8 W, duration of 1×10^{-7} s, and subjected along two meters to a modulating frequency of 1.2 GHz. The computation was performed at Z_e = 2 m using (FFT) algorithm.

Figure 2 shows that according to Equation (17), the normalized temporal distribution of the amplitude of the electric field of the phase-modulated laser pulse had a maximum power of 1.8 W, a duration of 1×10^{-7} s, and a modulating frequency of 1.2 GHz, when computed at Z = 10 m.

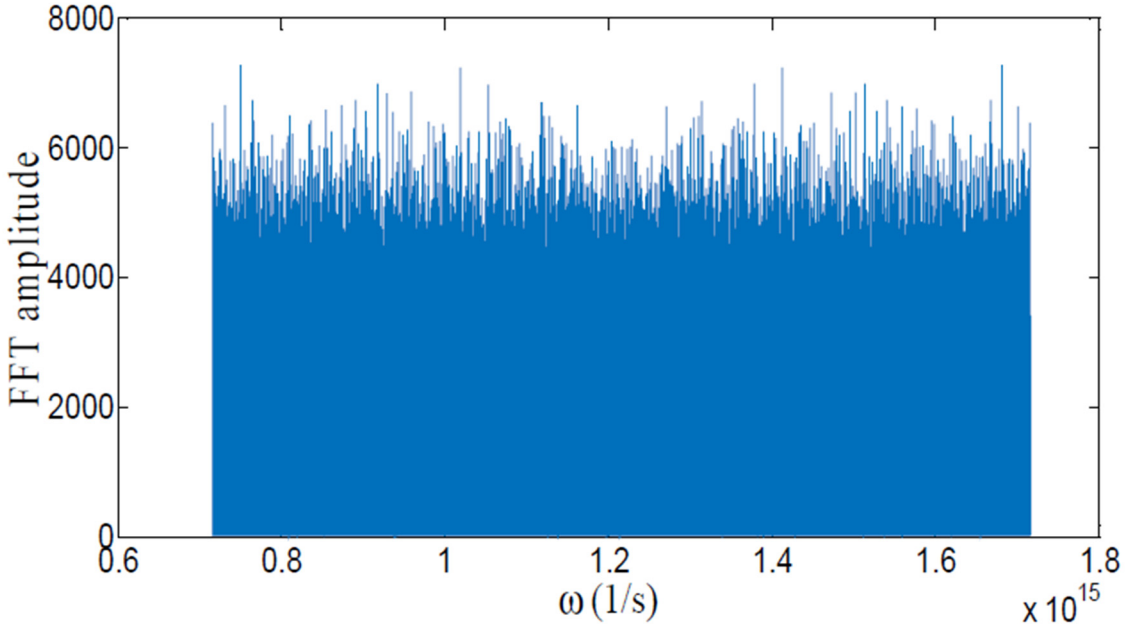

Figure 1. The modulus given in Au of the amplitude spectrum resulting from the (FFT) algorithm computed at Ze = 2 m for the electric-field amplitude of a laser pulse of input maximum power 1.8 W, duration of 1×10^{-7} s, and a modulating frequency of 1.2 GHz.

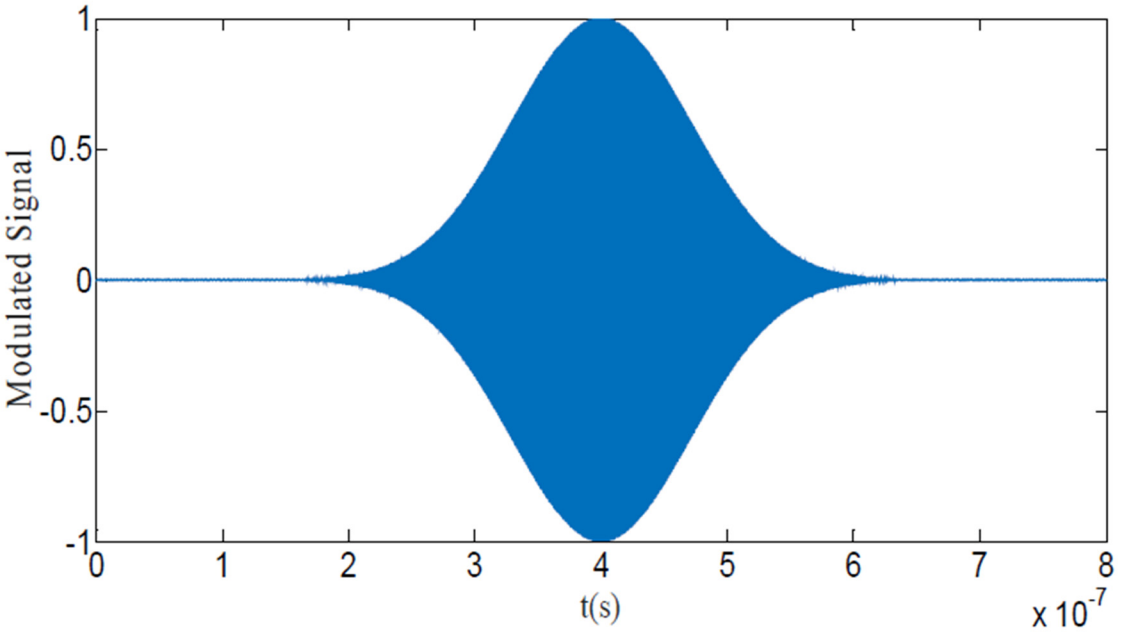

Figure 2. The normalized amplitude of the phase−modulated laser pulse of maximum power 1.8 W, duration 1×10^{-7} s computed at the end of the fiber z = 10 m and a modulating frequency 1.2 GHz.

2.2. Pulse Compression

To compress the spectral broadened laser pulse, it was directed into a combination of four prisms divided into two identical parallel sets (P1-P2 and P1′-P2′), as shown in Figure 3. The corresponding prisms of the two sets were located at the same x-positions and displaced in the *y*-axis. The first set acted as a Fourier transformer and was responsible for separating the frequency components comprising the pulse into parallel beams located at different y-positions. The second prism set acted as an inverse Fourier transformer and was

responsible for the spatial overlap of the spectral components throughout the environment outside the compressor.

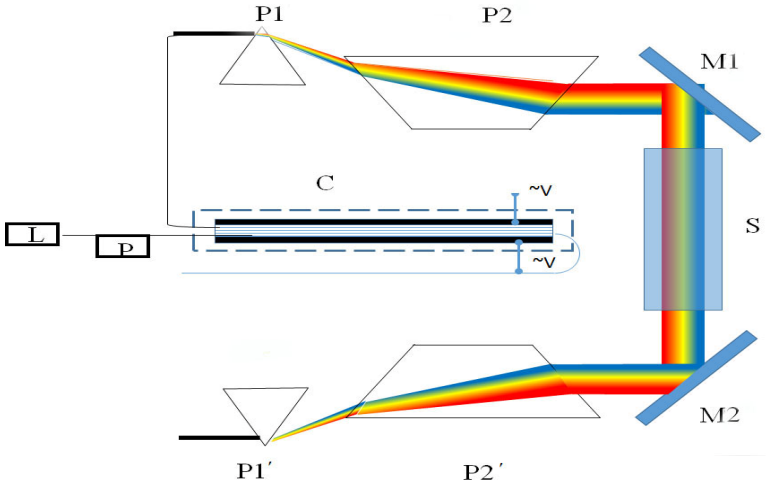

Figure 3. Overview of the compressor setup P1, P2, P1′, and P2′ are four prisms, L is a pulsed laser, P is a pump source, C is a capacitor M1 and M2 are mirrors and S is a slab subjected to a DC electric field.

The frequency components comprising the pulse that was emitted from the first prism set were directed via 45° mirror M1 onto the cross section of a slab. The slab, which had a low absorption coefficient as well as a well-defined frequency-dependent Kerr coefficient, was sandwiched between two electrodes. To change the spectral optical paths, each location across the width of the slab was subjected to a DC electric field with a constant value and a variable length in y-axis. This was realized, as shown in Figure 4, by connecting one of the two electrodes to the ground and the other to a DC electric source. The latter electrode was made from a photo-conducting material and was homogeneously illuminated with an array of LEDs. To change the phases of the spectral components, a stretchable computer-controlled opaque screen was used to control the illuminated area across the width of the slab. The emitted radiation from the slab was redirected by the mirror M2 into the lower set of prisms. The location of M2 was arranged such that the spectral components intersected the third prism P2′ at the same locations with respect to the base from which they were emitted from the second prism P2 of the upper set. Due to the symmetry of the configuration, the spectral components were overlapped at the output edge of the fourth prism and had the same slope. The slab's length was chosen so that the compressor would be approximately quadratic-shaped and the electric field across its thickness would have a moderate value. For all spectral components to be constructively superimposed at a desired location, the spectral phases had to be equal or shifted by multiple of 2π at that location. As shown in Figure 3, to fulfill this condition, the spectral optical path lengths across the setup and outside it had to be determined without subjecting the slab to an electric field. By dividing each of the obtained spectral optical path lengths by its corresponding vacuum wavelength (λ) and ignoring the integer number, a dimensionless fraction of the spectral wavelength was obtained. The corresponding phase of this fraction was obtained as follows:

$$\varphi(\Omega) = 2\pi \times \text{Fraction}(\lambda), \tag{18}$$

and the spectral angle $\Delta\varphi(\Omega)$ for completing $\varphi(\Omega)$ to 2π was:

$$\Delta\varphi(\Omega) = 2\pi - \varphi(\Omega). \tag{19}$$

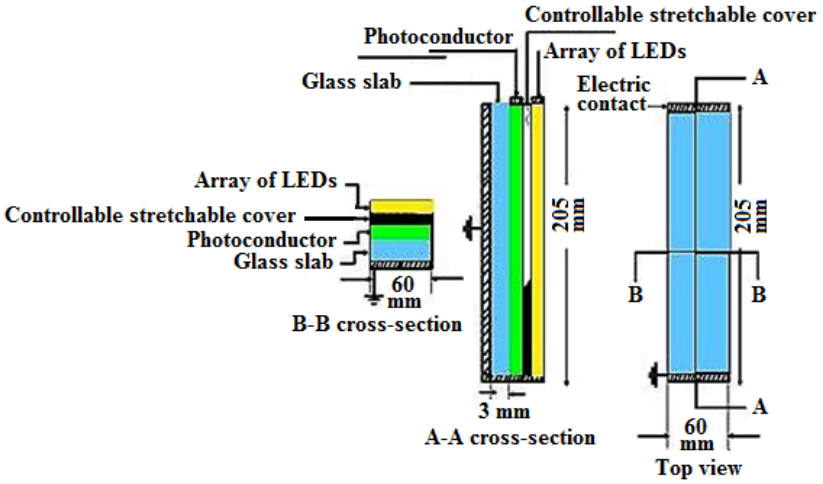

Figure 4. Overview of cross-sections in the slab responsible for stimulating the spectral phases to be in phase at any desired location.

To account for $\Delta\varphi(\Omega)$, as found in Equation (19), the nonlinear part of the refractive index of the slab's material, given in Equation (1), was activated. This was realized by subjecting a particular length $l(\Omega)$ along the slab at the location corresponding to the frequency across the slab's width to a DC electric field, according to:

$$\Delta\varphi(\Omega) = \frac{2\pi}{\lambda} n_2 E^2 l(\Omega) \tag{20}$$

Solving Equation (20) for $l(\Omega)$, one obtains

$$l(\Omega) = \frac{\Delta\varphi(\Omega)\lambda}{2\pi\, n_2 E^2} = \frac{\Delta\varphi(\Omega)\, c}{\Omega n_2 E^2}, \tag{21}$$

where n_2 is the nonlinear Kerr coefficient of the slab's material that was chosen to be the same as that of the fiber's material, $l(\Omega)$ is the length along the slab corresponding to the frequency Ω that was subjected to the DC electric field, and c is the vacuum velocity of light.

To simulate the temporal distribution resulting from the compressor at a desired location, an inverse fast Fourier transform (IFFT) algorithm was applied on the manipulated spectral phases.

2.2.1. Computations

The computation for determining $l(\Omega)$ given in (21) was performed for equilateral prisms of side length l_1 = 0.22 m, height as h = 0.19 m, length between the end of the base of the first prism and the apex of the second one as l_2 = 0.05 m, slab length as 0.2 m, slab thickness as 0.003 m, and electric field influencing the slab as 100 V/mm.

2.2.2. Results and Discussion

Figure 5 shows the fitted curve of the spectral length $l(\Omega)$ subjected to the DC electric field that influenced the slab to stimulate the frequency components to be in-phase at the desired location. The computation was carried out for a bandwidth of 10^{15} 1/s induced by modulating the pulsed laser phase by a frequency 1.2 GHz.

Figure 6 represents the compressed laser pulses computed for the modulating frequencies of 100 MHz and 1.2 GHz. For each of the modulating frequencies, the computation was performed for a fixed number of frequency samples 8×10^6. The results showed that the compression for the modulation frequency at 100 MHz was better than that found at 1.2 GHz. This behavior was due to the larger ratio of the selected frequencies relative to the actual frequencies at 100 MHz compared to that at 1.2 GHz. This may be attributed to the

fact that 1.2 GHz were more under-sampled or strongly aliased. In practical application, all frequencies would be in-phase if the slab is subjected to the desired distribution of the electric field given by $l(\Omega)$. Therefore, in this case, it was suggested that much better compression would be achieved.

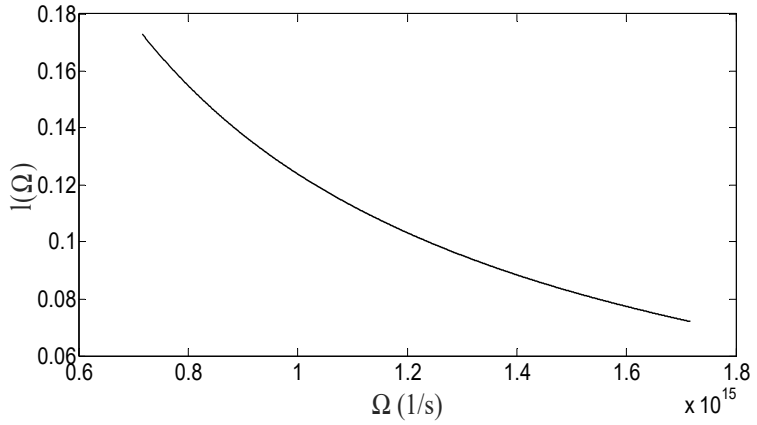

Figure 5. The fitted curve of the slab's length $l(\Omega)$ subjected to a DC electric-field distribution across the slab's width to equalize the phases of the spectral components of the broadened laser pulse at any desired location considering a laser with a pulse duration of 10^{-7} s, maximum power of 1.8 W, and phase modulated with a frequency of 1.2 GHz.

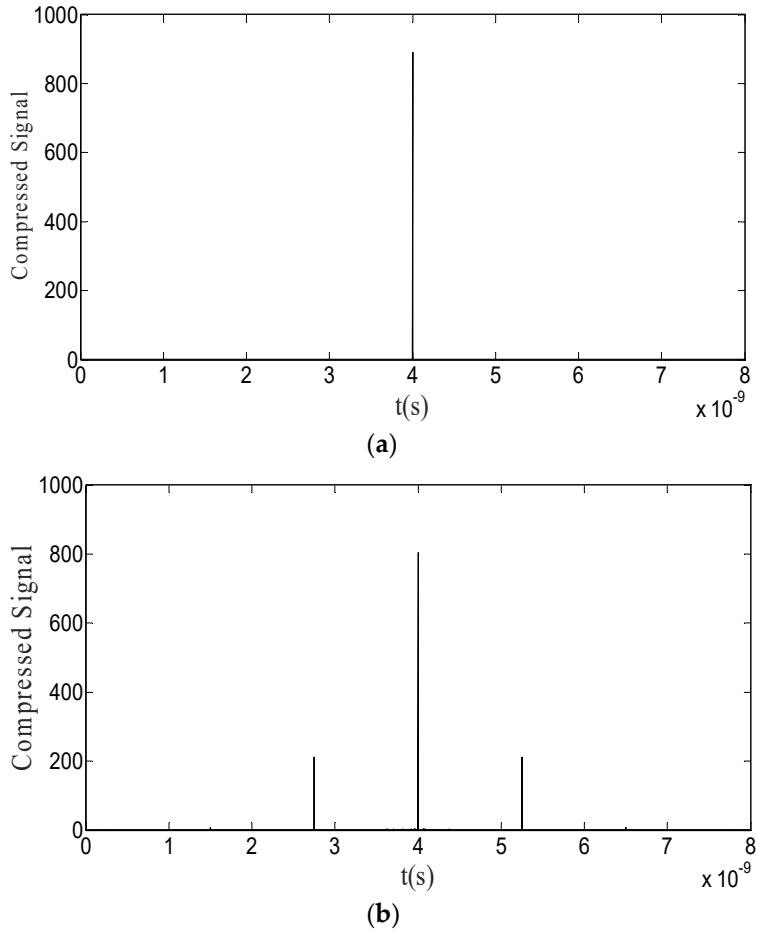

Figure 6. The compressed laser pulses for modulating frequencies (**a**) 100 MHz and (**b**) 1.2 GHz.

3. Conclusions

Although this proposal allowed an ordinary femtosecond laser to be generated, it differed from previous studies in the following respects. The pulses to be compressed were obtained from a mode-locked laser of moderate halfwidth and low power, such that self-phase-modulation could not be initiated. The compression was achieved using a one-stage compressor. The compressed pulses were generated at any desired location without the movement of the compressor elements. Moreover, from the above, it is evident that the spectral broadening of the laser pulse as well as the spectral phase manipulation depend only on n_2E^2 that must be in the order of n_0. This condition can be easily achieved by the external variation of the electric field. Consequently, this model can be used for any frequency that is not markedly attenuated during propagation in the proposed setup.

Author Contributions: Conceptualization, M.H.A.-e., S.E.I.H.E. and A.M.A.-R.; methodology, M.H.A.-e. and S.E.I.H.E.; software, M.H.A.-e. and A.M.A.-R.; validation, M.H.A.-e., S.E.I.H.E., A.F.H. and A.M.A.-R.; writing—original draft preparation, M.H.A.-e. and A.M.A.-R.; writing—review and editing, M.H.A.-e. and A.F.H.; visualization, supervision, S.E.I.H.E. All authors have read and agreed to the published version of the manuscript.

Funding: This research received no external funding.

Informed Consent Statement: Not applicable.

Data Availability Statement: Not applicable.

Acknowledgments: We would like to thank Jala El-Azab, head of the Department of Engineering Applications of Lasers at the National Institute of Laser Enhanced Sciences, Cairo University, for her fruitful discussion.

Conflicts of Interest: The authors declare no conflict of interest.

Appendix A

To uncover the desired electric-field strength distribution necessary for spectral broadening the laser pulse, Maxwell's equations were solved:

$$\nabla \times H = \frac{\partial D}{\partial t} + J, \tag{A1}$$

Since the field is in the insulator, J will be set equal to zero to get with D = Ee

$$\nabla \times H = \frac{\partial D}{\partial t} = \varepsilon \frac{\partial E}{\partial t} \tag{A2}$$

$$\nabla \times E = -\frac{\partial B}{\partial t}$$

with B = μH

$$\nabla \times E = -\mu \frac{\partial B}{\partial t} \tag{A3}$$

where H = magnetic field strength

Considering E to be parallel to the normal of the area of the capacitor plates, and its radial component to be omitted, H will build concentric circles about the center of the capacitor. Due to the considered geometry, the Maxwell equations have to be rewritten in cylindrical coordinates as:

$$\frac{\partial E(r,t)}{\partial r} = \mu \frac{\partial H(r,t)}{\partial t} \tag{A4}$$

$$\frac{\partial H(r,t)}{\partial r} + \frac{1}{r} H(r,tr,t) = \varepsilon \frac{\partial E(r,t)}{\partial t} \tag{A5}$$

considering the fields to be sinusoidal in time such that $H(r,t) = \mathrm{Re}[H(r)e^{i\omega t}]$, $E(r,t) = \mathrm{Re}[E(r)e^{i\omega t}]$.

The time derivative of the fields gives

$$\frac{\partial H(r,t)}{\partial t} = i\omega H(r)e^{i\omega t} \tag{A6}$$

$$\frac{\partial E(r,t)}{\partial t} = i\omega E(r)e^{i\omega t} \tag{A7}$$

Substituting the obtained expression in Equations (A6) and (A7) in Equations (A4) and (A5), one obtains

$$\frac{\partial E(r)}{\partial r} = i\mu\omega H(r) \tag{A8}$$

$$\frac{\partial H(r)}{\partial r} + \frac{1}{r}H(r) = i\varepsilon\omega E(r) \tag{A9}$$

Since the above equations are coupled, to decouple them one has to differentiate Equation (A9) w.r.t. (r), to obtain

$$\frac{\partial^2 H(r)}{\partial r^2} + \frac{1}{r}\frac{\partial H(r)}{\partial r} - \frac{1}{r^2}H(r) = i\varepsilon\omega\frac{\partial E(r)}{\partial r} \tag{A10}$$

substituting for $\frac{\partial E(r)}{\partial r}$ in Equation(A10) from Equation (A8) one obtains,

$$\frac{\partial^2 H(r)}{\partial r^2} + \frac{1}{r}\frac{\partial H(r)}{\partial r} - \frac{1}{r^2}H(r) + \varepsilon\mu\omega^2 H(r) = 0 \tag{A11}$$

Differentiating Equation (A8) w.r.t. (r) one obtains

$$\frac{\partial^2 E(r)}{\partial r^2} = i\mu\omega\frac{\partial H(r)}{\partial r} \tag{A12}$$

Substituting for $\frac{\partial H(r)}{\partial r}$ and $H(r)$ in Equation (A9) from Equations (A12) and (A8), respectively, gives,

$$\frac{1}{i\mu\omega}\frac{\partial^2 E(r)}{\partial r^2} + \frac{1}{r}\frac{1}{i\mu\omega}\frac{\partial E(r)}{\partial r} - i\varepsilon\omega E(r) = 0 \tag{A13}$$

with $k^2 = \omega^2\varepsilon\mu$, Equations (A11) and (A13) after normalization can be, respectively, written as

$$\frac{\partial^2 H(r)}{\partial r^2} + \frac{1}{r}\frac{\partial H(r)}{\partial r} + \left(k^2 - \frac{1}{r^2}\right)H(r) = 0 \tag{A14}$$

$$\frac{\partial^2 E(r)}{\partial r^2} + \frac{1}{r}\frac{\partial E(r)}{\partial r} + k^2 E(r) = 0 \tag{A15}$$

With $kr = x$, $k\partial r = \partial x$, so $k = \frac{\partial x}{\partial r}$ and Equations (A14) and (A15) can be written as:

$$\frac{\partial^2 E(r)}{\partial x^2} + \frac{1}{x}\frac{\partial E(r)}{\partial x} + E(r) = 0 \tag{A16}$$

$$\frac{\partial^2 H(r)}{\partial x^2} + \frac{1}{x}\frac{\partial H(r)}{\partial x} + \left(1 - \frac{1}{x^2}\right)H(r) = 0 \tag{A17}$$

The solution of Equations (A16) and (A17) are according to [30] given by:

$$E(r) = AJ_0(kr) + A' Y_0(kr) \tag{A18}$$

$$H(r) = BJ_1(kr) + B' Y_1(kr) \tag{A19}$$

Since Y_0, Y_1 are second-kind Bessel functions of zero and first order, respectively, and have singularity at kr = 0, thus A' and B' must vanish, giving:

$$E(r) = AJ_0(kr)$$
$$H(r) = BJ_1(kr)$$

since $J_1(0) = 0$, then $H(0) = 0$.

To determine B, the Ampere's law has to be applied on the magnetic field distribution $H(r)$.

From the relation

$$H(r = a).2\pi a = \int \frac{\partial D}{\partial t} dS = I \text{ with } D = \varepsilon_0 \varepsilon_r.E$$

where I is complex amplitude of the current through the wire feeding the capacitor.

Setting $r = a$ in the right-hand side of Equation (A19) one obtains, after substituting in the left-hand side for $H(r = a)$ from the above relation

$$B = \frac{I}{2\pi a} \frac{1}{J_1(ka)}, \tag{A20}$$

and thus $H(r)$ can be written as

$$H(r) = \frac{I_0}{2\pi a} \frac{J_1(kr)}{J_1(ka)} \tag{A21}$$

To determine $E(r)$, the obtained equation of $H(r)$ and its derivative w.r.t (r) have to be substituted into Equation (A9). This gives:

$$E(r) = \frac{1}{i\omega\varepsilon} \left(\frac{I_0}{2\pi a} \frac{1}{J_1(ka)} \left(-\frac{k}{kr} J_1(kr) + kJ_0(kr) \right) + \frac{1}{r} \frac{I}{2\pi a} \frac{J_1(kr)}{J_1(ka)} \right)$$

$$E(r) = \frac{I_0 k}{i\omega\varepsilon(2\pi a) J_1(ka)} J_0(kr) \tag{A22}$$

$$\text{With, } A = \frac{I_0 k}{i\omega\varepsilon(2\pi a) J_1(ka)} \tag{A23}$$

The following relation is found

$$\frac{B}{A} = \frac{i\omega\varepsilon}{k}$$

Substituting for k from the relation $k = \omega\sqrt{\varepsilon\mu}$ it follows that

$$\frac{B}{A} = i \frac{1}{\sqrt{\varepsilon\mu}} \varepsilon = i\sqrt{\frac{\varepsilon}{\mu}}$$

$$B = i\sqrt{\frac{\varepsilon}{\mu}} A \tag{A24}$$

From the obtained spatial amplitude distributions of the electrical and magnetic fields, their spatial and time distributions are given by:

$$E(r, t) = \text{Re}[AJ_0(kr)e^{i\omega t}],$$

$$H(r, t) = \text{Re}[BJ_1(kr)e^{i\omega t}],$$

$$E(r, t) = |A|J_0(kr) \sin \omega t,$$

$$\text{and } H(r,t) = \sqrt{\frac{\varepsilon}{\mu}}|A|J_1(kr)\cos\omega t\,,$$

with

$$|A| = \frac{\tilde{I}k}{\omega\varepsilon(2\pi a)J_1(ka)}$$

Setting $|A| = A$, it follows that

$$E(r,t) = AJ_0(kr)\sin\omega t \tag{A25}$$

$$H(r,t) = \sqrt{\frac{\varepsilon}{\mu}}AJ_1(kr)\cos\omega t \tag{A26}$$

References

1. Dey, D.; Tiwari, A.K. Controlling Chemical Reactions with Laser Pulses. *ACS Omega* **2020**, *5*, 17857–17867. [CrossRef] [PubMed]
2. Ikeda, K.; Kotaki, H.; Nakajima, K. X-ray generation by femtosecond laser pulses and its application to soft X-ray imaging microscope. *AIP Conf. Proc.* **2002**, *634*, 268–275. [CrossRef]
3. Afshari, M.; Krumey, P.; Menn, D.; Nicoul, M.; Brinks, F.; Tarasevitch, A.; Sokolowski-Tinten, K. Time-resolved diffraction with an optimized short pulse laser plasma X-ray source. *Struct. Dyn.* **2020**, *7*, 014301. [CrossRef]
4. Abbas, A.M.; Pan, Q.; Mandon, J.; Cristescu, S.M.; Harren Frans, J.M.; Khodabakhsh, A. Time-resolved mid-infrared dual-comb spectroscopy. *Sci. Rep.* **2019**, *9*, 17247. [CrossRef] [PubMed]
5. Borgwardt, M.; Omelchenko, S.T.; Favaro, M.; Plate, P.; Hohn, C.; Abou-Ras, D.; Schwarzburg, K.; van de Krol, R.; Atwater, H.A.; Lewis, N.S.; et al. Femtosecond time-resolved two-photon photoemission studies of ultrafast carrier relaxation in Cu_2O photoelectrodes. *Nat. Commun.* **2019**, *10*, 2106. [CrossRef]
6. Subramaniam, T.K. Erbium Doped Fiber Lasers for Long Distance Communication Using Network of Fiber Optics. *Am. J. Opt. Photonics* **2015**, *3*, 34–37. [CrossRef]
7. Ono, M.; Hata, M.; Tsunekawa, M.; Nozaki, K.; Sumikura, H.; Chiba, H.; Notomi, M. Ultrafast and energy-efficient all-optical switching with graphene-loaded deep-subwavelength plasmonic waveguides. *Nat. Photonics* **2019**, *14*, 37–43. [CrossRef]
8. Mottay, E.; Liu, X.; Zhang, H.; Mazur, E.; Sanatinia, R.; Pfleging, W. Industrial applications of ultrafast laser processing. *MRS Bull.* **2016**, *41*, 984–992. [CrossRef]
9. Alio, J.L.; AAbdou, A.A.; Puente, A.A.; Zato, M.A.; Nagy, Z. Femtosecond Laser Cataract Surgery: Updates on Technologies and Outcomes. *J. Refract. Surg.* **2014**, *30*, 420–427. [CrossRef] [PubMed]
10. Karasawa, N.; Morita, R.; Shigekawa, H.; Yamashita, M. Generation of intense ultrabroadband optical pulses by induced phase modulation in an argon-filled single-mode hollow waveguide. *Opt. Lett.* **2000**, *25*, 183–185. [CrossRef]
11. Hanna, M.; Delen, X.; Lavenu, L.; Guichard, F.; Zaouter, Y.; Druon, F.; Georges, P. Nonlinear temporal compression in multipass cells: Theory. *J. Opt. Soc. Am.* **2017**, *34*, 1340–1347. [CrossRef]
12. Weidner, P.; Penzkofer, A. Spectral broadening of picosecond laser pulses in optical fibres. *Opt. Quantum Electron.* **1993**, *25*, 1–25. [CrossRef]
13. Lu, C.-H.; Witting, T.; Husakou, A.; Vrakking, M.; Kung, A.H.; Furch, F.J. Sub-4 fs laser pulses at high average power and high repetition rate from an all-solid-state setup. *Opt. Express* **2018**, *26*, 8941–8956. [CrossRef] [PubMed]
14. Saleh, M.F.; Biancalana, F. Soliton dynamics in gas-filled hollow-core photonic crystal fibers. *J. Opt.* **2016**, *18*, 013002. [CrossRef]
15. Schmidt, B.E.; Béjot, P.; Giguère, M.; Shiner, A.; Trallero, C.; Bisson, E.; Kasparian, J.; Wolf, J.-P.; Villeneuve, D.; Kieffer, J.-C.; et al. Compression of 1.8 μm laser pulses to sub two optical cycles with bulk material. *Appl. Phys. Lett.* **2010**, *96*, 121109. [CrossRef]
16. Vuong, L.T.; Lopez-Martens, R.B.; Hauri, C.P.; Ruchon, T.; L'Huillier, A.; Foster, M.A.; Gaeta, A.L. Optimal pulse compression via sequential filamentation. In Proceedings of the Quantum Electronics and Laser Science Conference, Baltimore, ML, USA, 6–11 May 2007; p. JWE1.
17. Liao, K.-H.; Chen, M.-Y.; Flecher, E.; Smirnov, V.I.; Glebov, L.B.; Galvanauskas, A. Large-aperture chirped volume Bragg grating based fiber CPA system. *Opt. Express* **2007**, *15*, 4876–4882. [CrossRef] [PubMed]
18. Chauhan, V.; Bowlan, P.; Cohen, J.; Trebino, R. Single-diffraction-grating and grism pulse compressors. *Opt. Soc. Am.* **2010**, *27*, 619–624. [CrossRef]
19. Akturk, S.; Gu, X.; Kimmel, M.; Trebino, R. Extremely simple single-prism ultrashort-pulse compressor. *Opt. Express* **2006**, *14*, 10101–10108. [CrossRef] [PubMed]
20. Dombi, P.; Yakovlev, V.S.; O'Kee, K.; Fuji, T.; Lezius, M.; Tempea, G. Pulse compression with time-domain optimized chirped mirrors. *Opt. Express* **2005**, *13*, 10888–10894. [CrossRef]
21. Schulte, J.; Sartorius, T.; Weitenberg, J.; Vernaleken, A.; Russbueldt, P. Nonlinear pulse compression in a multi-pass cell. *Opt. Lett.* **2016**, *41*, 4511–4514. [CrossRef] [PubMed]
22. Nada, Y.S.; El-azab, J.M.; Othman, H.A.; Mohamad, T.; Maize, S.M.A. Interaction between Self Phase Modulation and Positive Group Velocity Dispersion in PMMA Polymer for Simplified Thin Film Compressor of High-Intensity Ultrashort Laser Pulses. *Nonlinear Opt. Quantum Opt.* **2020**, *52*, 299–311.

23. Shank, C.V.; Fork, R.L.; Yen, R.; Stolen, R.H. Compression of femtosecond optical pulses. *Appl. Phys. Lett.* **1982**, *40*, 761–763. [CrossRef]
24. Nikolaus, B.; Grischkowsky, D. 12× pulse compression using optical fibers. *Appl. Phys. Lett.* **1982**, *42*, 117–121. [CrossRef]
25. Tomlinson, W.J.; Stolen, R.H.; Shank, C.V. Compression of optical pulses chirped by self-phase modulation in fibers. *J. Opt. Soc. Am. B* **1984**, *1*, 139–149. [CrossRef]
26. Mével, E.; Tcherbakoff, O.; Salin, F.; Constant, E. Extracavity compression technique for high-energy femtosecond pulses. *J. Opt. Soc. Am. B* **2003**, *20*, 105–108. [CrossRef]
27. Jiménez, M.A.B.; Kuzin, E.A.; Ibarra-Escamilla, B.; Flores-Rosas, A. Optimization of the two-stage single-pump erbium-doped fiber amplifier with high amplification for low frequency nanoscale pulses. *Opt. Eng.* **2007**, *46*, 125007. [CrossRef]
28. Quintela, M.A.; Quintela, C.; Lomer, M.; Madruga, F.J.; Conde, O.M.; Lopez-Higuera, J.M. Comparison between a symmetric bidirectional-pumping and a unidirectional-pumping configurations in an erbium fiber ring laser. *Int. Soc. Opt. Eng.* **2007**, *6619*, 440–443.
29. Milonni, P.W.; Eberly, J.H. *Introduction to Nonlinear Optics*, 2nd ed.; John Wiley Sons, Inc.: Hoboken, NJ, USA, 2010; Chapter 10.
30. Bronshtein, I.N.; Semendyayev, K.A.; Musiol, G.; Muehlig, H. *Handbook of Mathematics*, 5th ed.; Springer: Berlin/Heidelberg, Germany, 2007.
31. Qian, S.; Li, J.; Zhang, Y. Absorptive Nonlinearity in Er-Doped Optical Fiber. *Wuhan Univ. J. Nat. Sci.* **1999**, *4*, 175–178. [CrossRef]
32. Fleming, J.W.; Wood, D.L. Refractive index dispersion and related properties in fluorine doped silica. *Appl. Opt.* **1983**, *22*, 3102–3104. [CrossRef]